Attorney's Docket No. 017750-507

IN THE UNITED STATES PATENT AND TRADEMARK OFFICE

In re Patent Application of	
Mark Myers et al.	Group Art Unit: 2878
Application No.: 09/988,660	Examiner: Shun K. Lee
Filed: November 20, 2001	Appeal No.:
For: MULTIBAND SINGLE ELEMENT WIDE FIELD OF VIEW INFRARED IMAGING SYSTEM	

APPEAL BRIEF

Mail Stop APPEAL BRIEF - PATENTS
Commissioner for Patents
P.O. Box 1450
Alexandria, VA 22313-1450

Sir:

This appeal is from the decision of the Primary Examiner dated March 23, 2005 (Paper No. 0305), finally rejecting claims 4, 6 and 9-20, which are reproduced as the Claims Appendix of this brief.

☒ A check covering the ☐ $250.00 (2402) ☒ $500.00 (1402) Government fee is filed herewith.

☐ Charge ☐ $250.00 (2402) ☐ $500.00 (1402) to Credit Card. Form PTO-2038 is attached.

The Commissioner is hereby authorized to charge any appropriate fees under 37 C.F.R. §§1.16, 1.17, and 1.21 that may be required by this paper, and to credit any overpayment, to Deposit Account No. 02-4800.

09/16/2005 JADD01 00000096 09988660
01 FC:1402 500.00 OP

Table of Contents

I. Real Party in Interest

Lockheed Martin Corporation is the real party in interest, and is the assignee of Application No. 09/988,660.

II. Related Appeals and Interferences

The Appellants' legal representative, or assignee, does not know of any other appeal or interferences which will affect or be directly affected by or have bearing on the Board's decision in the pending appeal.

III. Status of Claims

Pending claims 4, 6 and 9-20 are appealed in this application. Claim 4 is the only independent claim. Claims 6 and 9-20 depend from claim 4.

Claims 4, 9-13 and 15-20 stand rejected under 35 U.S.C. §103(a) as being unpatentable over U.S. Patent No. 4,507,551 to Howard et al. (hereafter "*Howard et al.*") in view of Applicant's Admitted Prior Art, U.S. Patent No. 5,369,511 to Amos (hereafter "*Amos*") and U.S. Patent Application Publication No. 2001/0029816 to Ben-Menachem et al. (hereafter "*Ben-Menachem et al.*"); and claims 6 and 14 stand rejected under 35 U.S.C. §103(a) as being unpatentable over *Howard et al.* in view of Applicant's Admitted Prior Art, *Amos* and *Ben-Menachem et al.* and further in view of U.S. Patent No. 6,034,407 to Tennant et al. (hereafter "*Tennant et al.*").

IV. Status of Amendments

All amendments in this application have been entered.

V. Summary Claimed Subject Matter

The present application relates generally to infrared imaging systems. Exemplary embodiments of the disclosed infrared imaging system are illustrated in Figures 1 and 2, reproduced and discussed below.

Figure 1 shows a schematic perspective view of the infrared imaging system 100 having a compressor housing 102 and an optical housing 104. The optical housing 104 has a cryogenic subassembly 106, an optical subassembly 108 and an electronics subassembly 110. The optical subassembly 108 is positioned within the cold space 116 of the cryogenic subassembly 106 at the receiving end 118 of the optical housing 104. A lens 122 and infrared (IR) detector 124 are included in the optical subassembly 108.

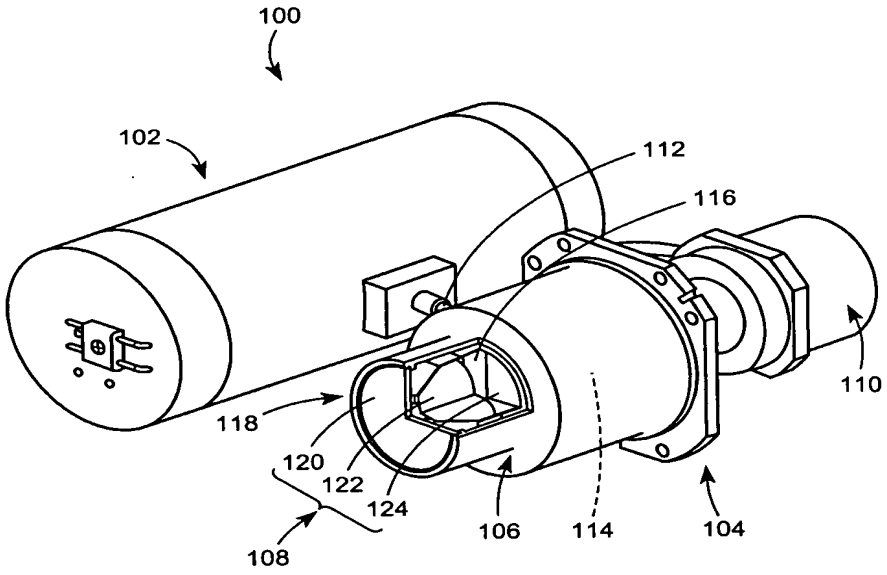

FIG. 1

Figure 2 shows a plan cross-sectional schematic view of the optical subassembly 200, with the lens 206 positioned in the cold space 210. The lens receives incident IR energy 218 through an IR transmissive window and projects the IR energy to a detector 208.

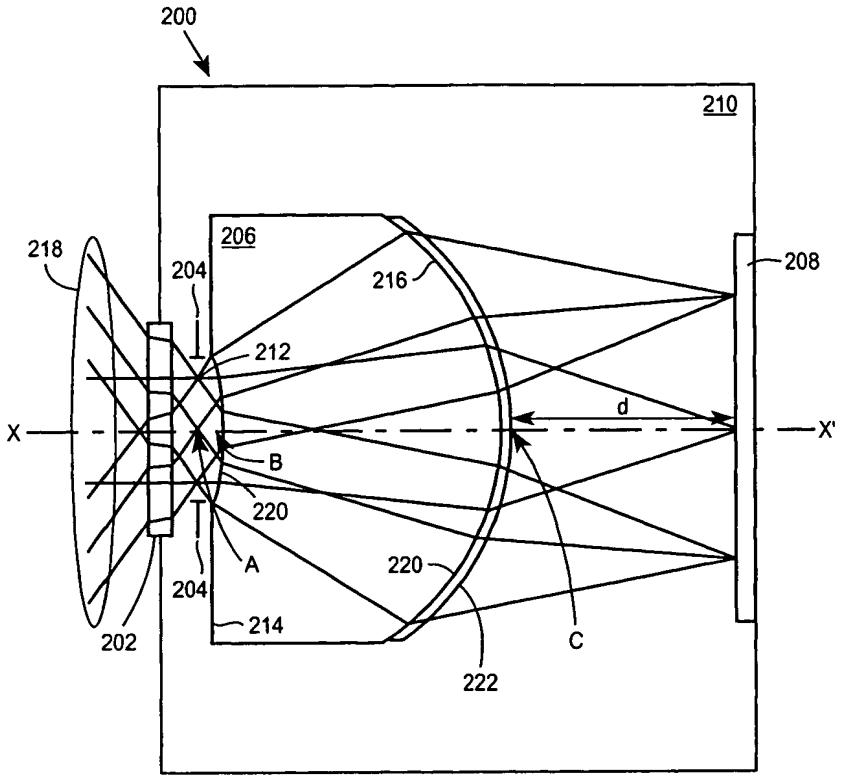

FIG. 2

The lens has a first surface with specific features and optical elements designed to manipulate the IR energy in a desired manner.

For example, the first and second surfaces 214, 216 of the lens 206 are aspherical over at least a portion of the lens 206 and such that the aspherical surfaces 220 are aligned radially symmetric in the transmission path about axis X-X'. Alternatively, the entire first or second surface 214, 216 may be aspherical. However, the cross-section of the caustic at the points B, C is no greater than the surface area of the first or second surface 214, 216 and is such that the transmission path may propagate through the aspherical surfaces 220.

In addition to being aspherical, the second surface 216 of the lens 206 is also a holographic optical element (HOE) 222, alternatively called a binary surface or a diffractive grating on a curved surface. The HOE 222 uses principles of harmonics to discriminate and propagate a plurality of wavelengths.

Typically, a HOE design starts with picking a center or design wavelength. In the present application, the design is based around two center wavelengths. While the two wavelengths have a relationship consistent with the diffractive orders, the lens design technique used to create the HOEs configured two HOEs (each with a different design wavelengths, e.g., with the ranges of 3-5 μm or 8-12 μm) but placed them in the same physical location, thus creating a single HOE with two design wavelengths.

Accordingly, exemplary embodiments of the HOE 222 discriminate and propagate at least two wavelengths. For example, a first wavelength is manipulated by the HOE 222, a second wavelength, which is a harmonic component of the first wavelength, is also manipulated by the HOE 222. The principles also apply to all subsequent wavelengths to be manipulated by the HOE 222.

In the present application, the optical elements of the first and second aspherical surfaces 214,216, e.g., the aspherical surfaces and the HOE, combine to manipulate infrared energy from at least two wavebands in the infrared spectrum. In one embodiment, a first waveband has a wavelength of 3-5 μm, preferably 4-4.5 μm, and a second waveband has a wavelength of 8-12 μm, preferably 8.5-9.5 μm. In a second embodiment, the first and second aspherical surfaces 214,216, the HOE 222, and the detector 208 combine to manipulate infrared energy from at least two wavebands in the infrared spectrum

As shown in Figure 2, a detector 208 is positioned in alignment with the other components of the optical subassembly 200 about the axis X-X' at a focal length distance d from the second surface 216 of the lens 206, at a coincident focal plane to at least two wavelengths manipulated and transmitted by the lens 206 and the holographic optical element (HOE) 222. The detector 208 can discriminate at least two or more wavelengths of incident energy in the IR spectrum, such as wavelengths at 3-12 μm. The detector 208 processes the wavelengths to produce multiple waveband detection capability within a single detector. In an exemplary embodiment, the detector 208 concurrently collects radiation from multiple, adjacent spectral radiation bands. This type of detector may be used in "hyperspectral imaging."

Several advantages of the exemplary infrared imaging system 100 are disclosed at paragraphs [0035] to [0037].

For example, use of a single, color corrected element in the dewar provides an optical subassembly that is shorter and provides for a better form factor and lower part count for the entire infrared imaging system. Also, by enclosing the single lens within the detector dewar, the optical subassembly, including the optical stop, lens and detector, are all located within a single enclosure. Previously, tight alignment tolerances had to be maintained across the detector-to-dewar mount, the dewar-to-optical housing mount and the optical housing-to-optics mount. By eliminating the multiple interfaces the total tolerance budget can be applied on the single interface, reducing the required manufacturing and assembly tolerances and reducing the requirement for precision alignment across multiple interfaces.

In another example, placing the single, color corrected lens 206 in the cryogenic subassembly 106 is advantageous because it places the optical subassembly 200 in a controlled temperature environment. By maintaining the lens 206 at a nearly constant temperature, the need for a passive or active athermalization system to correct the thermally induced focus variations may be eliminated. While this could be accomplished previously by heating or cooling the optics with a separate device, this approach makes use of the cooling capabilities that are already present in the system. Also, enclosing the optical subassembly 200 in the cryogenic subassembly 106 places the optics in a sealed, evacuated environment, protecting it against dust or other contamination. While this could be accomplished in a separate enclosure, this approach makes use of capabilities already present in the optical housing 104.

In addition, the alignment of the optical components permits a detector to be located at the focal plane for the lens system. In previous multi-lens imaging systems, it was difficult to ensure alignment of the optical components because the thermal coefficient of expansion resulted in disparate movement of the individual optical components. A unitary structure housed within the cold space essentially eliminates thermal transients amongst the components once a temperature equilibrium has been achieved by the cryogenic housing and compressor, thereby overcoming the alignment problems.

The foregoing features also permit the design of a lower cost system with the same performance capabilities of current, more expensive ones.

VI. Grounds of Rejection to be Reviewed on Appeal

Whether the combination of disclosures in *Howard et al.,* Applicant's Admitted Prior Art, *Amos* and *Ben-Menachem et al.* as proposed by the Examiner renders claims 4, 9-13 and 15-20 obvious.

VII. Argument

Independent claim 4 stands rejected under 35 U.S.C. §103(a) as being unpatentable over the combination of disclosures in *Howard et al.,* Applicant's Admitted Prior Art, *Amos* and *Ben-Menachem et al.* on the grounds set forth in paragraphs 2-3 of the Official Action dated March 23, 2005. This rejection is respectfully traversed for at least the following reasons.

A. The holographic optical element of *Amos* does not function to correct the claimed wavelengths and therefore the rejection does not teach or suggest all elements of the claim.

Applicants claim specific structural features and arrangements, e.g., a single lens with a first aspheric profile and a second aspheric profile having, in addition, a holographic optical element, to obtain the desired result. The combinations of features contributes to both 1) color correct a first color band of infrared energy having wavelengths of 3 to 5 micrometer and 2) coincidently focus at the common focal plane the first color band and a second color band of infrared energy having wavelengths of 8 to 12 micrometers.

In the rejection, the Examiner relies upon the disclosure in *Amos*. Specifically, the Examiner points to the assertion of *Amos* that holographic optical elements (HOEs) are able to correct chromatic aberrations at all wavelengths (see, col. 18, lines 59-60). However, this disclosure in *Amos* is not consistent with the understanding in the art of the corrective capabilities of HOEs at the time and has, therefore, been misapplied to reject the claims. Further, when correctly interpreted,

this disclosure in *Amos*, in combination with the prior art of *Howard et al.* and *Ben-Menachem et al.* will not correctly image over multiple wavebands as claimed.

Amos describes the utility of a series of conical or pyramidal surfaces. One of the proposed methods of creating these cones and pyramids is with HOEs. In column 18, line 43 to column 19, line 9, *Amos* discusses the ability of HOEs in general. More specifically, HOEs are an implementation of *Amos's* canonical or pyramidal generators to correct chromatic aberrations. *Amos* states "However, binary optics techniques add a notched diffractive component to the refractive lens so that chromatic aberration is corrected." The "notched diffractive component" is the contribution of the standard HOE, which has a wavelength dependence and would require some additional method to correct all wavelengths of the electromagnetic spectrum. Thus, while *Amos* creates "a plethora of tiny staircase-type notches" (Column 19, lines 2-17), it is not a fundamental property of the HOE disclosed in *Amos* to correct all wavelengths of the electromagnetic spectrum.

To further illustrate and corroborate the above understanding of the properties of *Amos's* HOEs, Applicants submit herewith in Appendix IX portions of "Optical Design Fundamentals For Infrared Systems" by Max J. Riedl (SPIE Optical Engineering Press, 1995). The author discusses the properties of diffractive optics on pages 93-102 in the section titled "Diffractive (Binary) Optics." (The terms holographic, binary or diffractive are synonymous in optical surface design.)

Specifically referring to Figure 4.26, the use of diffractive surfaces to correct chromatic aberrations (as well as the combination of a HOE and a standard surface as mentioned by the Examiner) is shown. Note that, just like a standard optical surface, a diffractive surface has a variation of focus position with wavelength, indicated by the short and long image positions in the diagram. These short and long image positions can be balanced with the short and long image positions of a standard refractive surface to make a chromatically corrected image.

However, there are limitations to the correction of an HOE. The limitations are put forward in section 4.5.2 Diffraction Efficiency and 4.5.5 "Useful" Spectral Bandwidth. The "useful" bandwidth mentioned here is less than that obtained from the claimed infrared imaging apparatus. The corrections of an HOE could more

accurately be described as not increasing the bandwidth, but allowing for multiple bands.

Applying this understanding of the features and limitations of the HOE disclosed in *Amos*, it is respectfully asserted that the HOE of *Amos* cannot function to correct a first color band of infrared energy having wavelengths of 3 to 5 micrometer and coincidently focus at a common focal plane the first color band and a second color band of infrared energy having wavelengths of 8 to 12 micrometer as presently claimed. Rather, at best *Amos*, corrects multiple bands of energy that are much closer in wavelength than that claimed.

Part of the Examiner proposed combination also relies upon the disclosure in *Ben-Menachem et al.* *Ben-Menachem et al.* discloses a lens element with two aspheric surfaces. However, the disclosed lens element does not teach or suggest the presently claimed imaging apparatus.

Applying the above discussion on HOEs to the elements disclosed in *Ben-Menachem et al.*, it is respectfully asserted that the elements in *Ben-Menachem et al.* cannot correct a first color band of infrared energy having wavelengths of 3 to 5 micrometer and coincidently focuses at the common focal plane the first color band and a second color band of infrared energy having wavelengths of 8 to 12 micrometer as presently claimed. Rather, the elements in *Ben-Menachem et al.* operate on only one of the two claimed wavelength ranges. This interpretation of *Ben-Menachem et al.* is supported by the disclosure in *Ben-Menachem et al.* itself.

For example, *Ben-Menachem et al.* discloses at paragraph [0060], line 8, that when used in an IR thermal imaging system, the disclosed double aspheric lens operates in the 8-12 μm ***or*** the 3-5 μm wavelength range (***emphasis added***). In other words, the disclosure in *Ben-Menachem et al.* explicitly teaches that only one of the wavelength ranges manipulated by the presently claimed imaging apparatus is within the operating range of his apparatus. This is consistent with the above discussion of typical HOEs and the limitations to the correction of a typical HOE. Accordingly, this reference also does not contribute, alone or in combination with the other references, to teaching or suggesting the claim feature.

The other references in the proposed combination disclose other features of the claims and are not directed to, nor teach or suggest, features of the lens to

include the claimed color correction of a first color band of infrared energy having wavelengths of 3 to 5 micrometer and the claimed coincident focusing at the common focal plane the first color band and a second color band of infrared energy having wavelengths of 8 to 12 micrometers. Thus, these references are not discussed here. Rather, the prior discussion of these references is incorporated by reference.

For at least the above reasons, the rejection should be withdrawn because the combined disclosures do not teach or suggest all of the features of the present claims.

VIII. Claims Appendix

See attached Claims Appendix for a copy of the claims involved in the appeal.

IX. Evidence Appendix

See attached Evidence Appendix for a copy of portions of "Optical Design Fundamentals for Infrared Systems" by Max J. Riedl (SPIE Optical Engineering Press, 1995). This document has previously been submitted with the Response dated January 19, 2005.

Respectfully submitted,

Buchanan Ingersoll PC

Date September 15, 2005

By: _____
Jeffrey G. Killian
Registration No. 50,891

P.O. Box 1404
Alexandria, Virginia 22313-1404
(703) 836-6620

VIII. CLAIMS APPENDIX

The Appealed Claims

Claims 1 - 3 (Canceled)

4. (Previously Presented) An infrared imaging apparatus comprising:

a dewar, having an internal volume that defines a cold space;

an IR transmissive window that seals the cold space to receive IR energy directly from an IR source;

a first lens located within the cold space to receive IR energy directly from the IR transmissive window;

an IR detector located within the cold space in operational communication with the first lens and positioned coincident to a focal plane of at least a first and second wavelength of IR energy; and

an optical stop located within the cold space in front of the first lens,

wherein the first lens has a first aspheric profile on a first side and a second aspheric profile on a second side, the first side parallel to the second side and the second side facing the detector,

wherein the second aspheric profile has a holographic optical element, and

wherein the holographic optical element color corrects a first color band of infrared energy having wavelengths of 3 to 5 micrometer and coincidently focuses at the common focal plane the first color band and a second color band of infrared energy having wavelengths of 8 to 12 micrometer.

5. (Canceled)

6. (Previously Presented) The infrared imaging apparatus of claim 4, wherein the detector is a hyperspectral detector.

7. (Canceled)

8. (Canceled)

9. (Previously Presented) The infrared imaging apparatus of claim 4, wherein the holographic optical element coincidently focuses both the first color band of infrared energy and the second color band of infrared energy at a common focal plane.

10. (Previously Presented) The infrared imaging apparatus of claim 4, wherein one of the wavelengths of the second color band is a harmonic component of one of the wavelengths of the first color band.

11. (Previously Presented) The infrared imaging apparatus of claim 4, wherein the first lens is made of germanium.

12. (Previously Presented) The infrared imaging apparatus of claim 4, wherein the first lens is made of silicon.

13. (Previously Presented) The infrared imaging apparatus of claim 4, wherein the apparatus performs at an F-stop (F/#) of at least 1.4 with a square field of view of 90x90 degrees.

14. (Previously Presented) The infrared imaging apparatus of claim 4, wherein the detector concurrently collects radiation from multiple, adjacent spectral radiation bands.

15. (Previously Presented) The infrared imaging apparatus of claim 4, wherein the first aspheric surface has the following prescription:

radius = -0.94467;

k = 28.345216;

a = -2.13952;

b = -69.5274;

c = 2342.04;

d = -56841.9; and

first surface thickness = 0.548467.

16. (Original) The infrared imaging apparatus of claim 15, wherein the second aspheric surface has the following prescription:

radius = -0.61281;

k = 0.1399;

a = 0.033459;

b = -2.3598;

c = 10.889;

d = -36.331; and

second surface thickness = 0.462731.

17. (Original) The infrared imaging apparatus of claim 16, wherein the holographic optical element has the following prescription:

-0.0051393, -0.10212, 0.91035, -2.3946.

18. (Previously Presented) The infrared imaging apparatus of claim 4, wherein the first aspheric surface has the following prescription:

radius = -1.23508;

k = 36.049455;

a = -1.69104;

b = -98.6413;

c = 5589.83;

d = -162359; and

first surface thickness = 0.761661.

19. (Original) The infrared imaging apparatus of claim 18, wherein the second aspheric surface has the following prescription:

radius = -0.81270;

k = -0.10748;

a = 0.054475;

b = -0.72423;

c = 2.9155;

d = -7.8939; and

second surface thickness = 0.480234.

20. (Original) The infrared imaging apparatus of claim 19, wherein the holographic optical element has the following prescription:

-0.017112, -0.038991, 0.55069, -1.6405.

IX. EVIDENCE APPENDIX

Enclosed is a copy of portions of "Optical Design Fundamentals For Infrared Systems" by Max J. Riedl (SPIE Optical Engineering Press, 1995).

$$(f/\#)_{\text{effective}} = \frac{1}{\sqrt{1-\varepsilon^2}}(f/\#), \tag{4.34}$$

where ε is the ratio of the secondary and primary mirror diameters. In the case discussed $\varepsilon = 0.5$, which yields an effective (*f*/#) of 2.3. It is easy to see that the S/N will be reduced by 25%. If this is not acceptable, the initial (*f*/#) has to be lowered accordingly and the impact on the aberrations has to be reevaluated.

4.4.5 Instantaneous field of view

As we know, for a perfect optical system, the instantaneous field of view (IFOV) is strictly determined by the size of the detector element d'. Its angular extent is expressed as IFOV = $2u_p = d'/f$. The blur spot is at best the diffraction size of $B = 2.44\ \lambda\ (f/\#)$, but frequently larger, depending on the residual aberrations. In either case, one has to agree with the user on the energy percentage of the blur spot size that is acceptable for the application as a field cutoff.

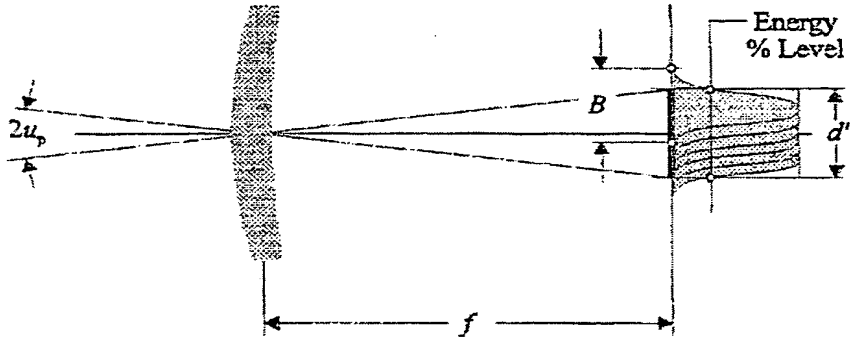

FIG. 4.23 Blur spot and instantaneous field of view.

4.5 Diffractive (Binary) Optics

As a practical matter, one can look at diffraction simply as another method besides refraction and reflection to change the direction of light rays. Fig. 4.24 shows the three different ways of redirecting rays by an optical element.

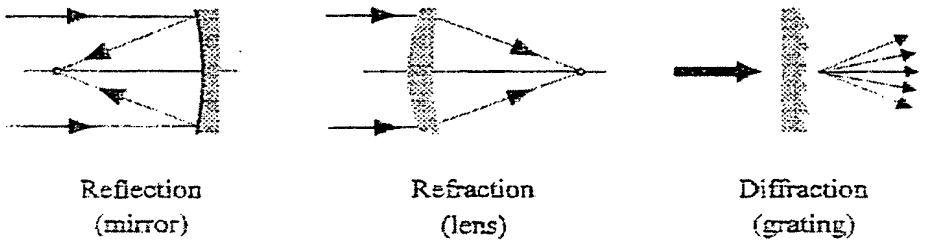

FIG. 4.24 Three ways to change direction of light rays

Usually, one thinks first of a linear grating as a diffractive element, because it has been in use for a long time. By arranging a diffractive phase profile properly as concentric rings on a flat substrate, the grating becomes a diffractive lens. Such a lens is sometimes referred to as a single-wave Fresnel lens because of the one-wave optical path difference that exists at the zone transitions.

4.5.1 The simple diffractive singlet

A diffractive singlet as shown in Fig. 4.25 consists of a plane-parallel disk with a circular grating structure imposed on one surface. The performing principle of this surface-relief structure lies in the periodic phase delay introduced by the continuous change of the physical thickness of the element according to the phase equation

$$\phi(r) = \frac{2\pi}{\lambda_0}(ar^2 + br^4 + cr^6 + \quad) \tag{4.35}$$

In this equation, a, b, c, etc., are the phase coefficients, λ_0 is the wavelength, and r is the radial coordinate. Diffractive zone boundaries occur at each 2π transition. The maximum zone depth at the transition is

$$d_{max} = \frac{\lambda_0}{N_0 - 1} \tag{4.36}$$

N_0 is the refractive index of the lens material at the design wavelength λ_0.

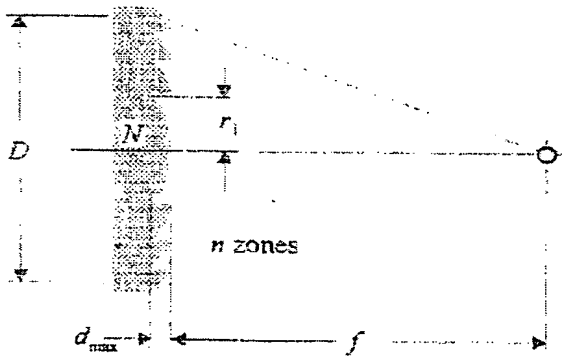

FIG. 4.25 Cross section of simple diffractive lens (single-wave Fresnel lens)

The location of the zones in a diffractive lens can be determined from the equation for the classical Fresnel zone plate with

$$r_n = \sqrt{2n\lambda_0 f + n^2\lambda_0^2} \tag{4.37}$$

If $f \gg n\lambda_0$, $\quad r_n \cong \sqrt{2n\lambda f}$. (4.38)

where n is the zone number. Therefore, the first zone radius $r_1 \cong \sqrt{2\lambda_0 f}$ and $r_n \cong r_1\sqrt{n}$, from which we derive the total number of zones required for a lens with a diameter D.

$$n_{\text{total}} \cong \left(\frac{D}{2r_1}\right)^2. \tag{4.39}$$

Eq. (4.39) indicates that the required zone number for a diffractive lens is independent of the chosen substrate material.

Based on the quadratic term of the phase equation [Eq. (4.35)], $r_1 = \sqrt{\lambda_0/a}$, which leads to the relation $2\lambda_0 f = \lambda_0/a$, or

$$a = -\frac{1}{2f}. \tag{4.40}$$

The minus sign indicates the direction of the phase profile.

For a lens with a focal length of $f = 80$ mm and a diameter of $D = 16$ mm, used in the infrared spectrum at a wavelength of $\lambda_0 = 4$ μm, we find:

$a = -0.00625$ mm^{-1}, $r_1 = 0.8$ mm, and $n_{\text{total}} = 100$ zones.

$r_2 = 1.131$ mm
$r_3 = 1.386$ mm

etc.

$r_{99} = 7.960$ mm
$r_{100} = 8.00$ mm.

The zone spacing at the edge of the lens has diminished from the spacing of 0.8 mm for the first zone to 0.04 mm. This is an important indicator for the manufacturing process to be chosen.

As a quick reference approximation, the minimum zone spacing is stated by

$$(\Delta r)_{\min} \cong 2\lambda_0\left(f/\frac{\#}{}\right). \tag{4.41}$$

If we select silicon, a suitable material for $\lambda_0 = 4$ μm, where its index $N_0 = 3.425$, the maximum zone depth $d_{\max} = 1.65$ μm.

4.5.2 The hybrid achromat

For many applications, especially for broadband systems in the infrared region, the hybrid achromat presents a very interesting alternative to the conventional doublet.[5] By combining refractive and diffractive powers, one can effectively correct the chromatic

aberration. The basic principle for this correction lies in the fact that a diffractive lens focuses the longer wavelengths closer to the lens than the shorter wavelengths. As indicated in Fig. 4.26, this is just the opposite of the behavior of a refractive lens. The total power of the refractive/diffractive combination is the sum of the powers of the elements.

$$\phi_{\text{hybrid}} = \phi = \phi_{\text{refractive}} + \phi_{\text{diffractive}} \tag{4.42}$$

or

$$f = \frac{f_r f_d}{f_r + f_d} \qquad \text{with} \quad f = \frac{1}{\phi} \tag{4.43}$$

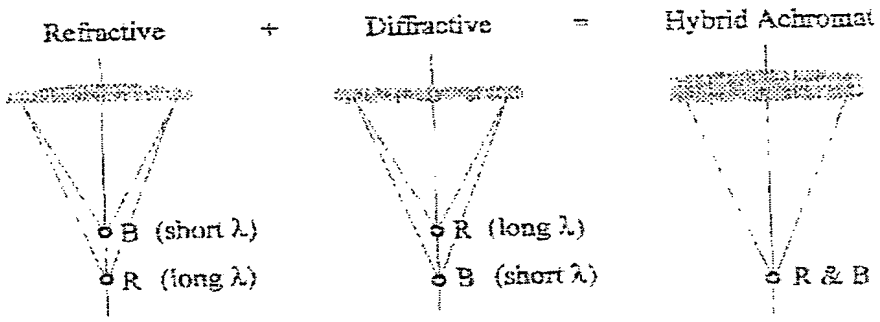

FIG. 4.26 Principle of combining refractive and diffractive powers for color correction.

By assigning the proper power to each element, their individual chromatic contributions cancel.

The following conditions must exist to achieve the correction:

$$f_r = \left(1 - \frac{V_d}{V_r}\right) f , \tag{4.44}$$

and

$$f_d = \left(1 - \frac{V_r}{V_d}\right) f . \tag{4.45}$$

with

$$V_r = \frac{N_0 - 1}{N_S - N_L} \qquad \text{and} \qquad V_d = \frac{\lambda_0}{\lambda_S - \lambda_L} ,$$

where V_r is the Abbe number for refraction, V_d is the Abbe number for diffraction, λ_0 is the center wavelength for which the index of refraction is N_0, and λ_S and λ_L are the short- and long-wavelength limits of the spectral band. Notice that V_d is independent of any material used for the lens.

With these relationships, it becomes quite simple to estimate quickly, based on the first term (the quadratic term) of the phase equation [Eq. (4.35)], what the first zone radius will be and how many zones are needed for a particular lens.

$$r_1 = \sqrt{2\lambda_0 f_d}. \tag{4.46}$$

$$n_{\text{total}} = \left(\frac{D}{2r_1}\right)^2. \tag{4.47}$$

4.5.3 Numerical examples

To correct an *f*/1, 100-mm-focal-length germanium lens used in the 8–12μm region, for which we select 10 μm as the center wavelength, we find that ν_r = 990, ν_d = -2.5, f_r = 100.253 mm, and f_d = 39,700 mm. Further, r_1 = 28.178 mm, n_{total} = 4, with r_2 = 39.450 mm, and r_3 = 48.806 mm. The fourth zone ends at the edge of the lens, where r_{max} = 50 mm. The maximum depth of the zones at their transitions is d_{max} = 3.33 μm.

From the equations we can see that large Abbe numbers and long wavelengths result in low zone numbers, as demonstrated with the example. This very favorable characteristic exists for most common materials used in the mid- and long-IR wavelengths regions. A phase profile with only a few zones can be very economically machined by single-point diamond turning.[5]

For a quick reference, Figs. 4.27 and 4.28 show nomograms covering achromatic hybrids for the 3- to 5- and 8- to 12-μm windows. Only materials that can be diamond-turned have been included in these nomograms.

In Fig. 4.27 a ZnSe lens with 50-mm focal length *f* is investigated. The first zone radius r_1 = 6 mm. For a lens diameter of D = 50 mm (*f*/1), the total zone number required to correct chromatic aberration is found to be $n_{\text{total}} \equiv 17$. Table 4.1 lists all the numerical values of the zone radii for the lens discussed.

Table 4.1 Zone radii for *f*/1 ZnSe example lens.

Zone n	Radius r	Zone n	Radius r
1	6.000 mm	10	18.974 mm
2	8.485	11	19.900
3	10.392	12	20.785
4	12.000	13	21.633
5	13.416	14	22.450
6	14.697	15	23.238
7	15.875	16	24.000
8	16.971	17	24.739
9	18.000	18	25.456 (D/2 = 25 mm)

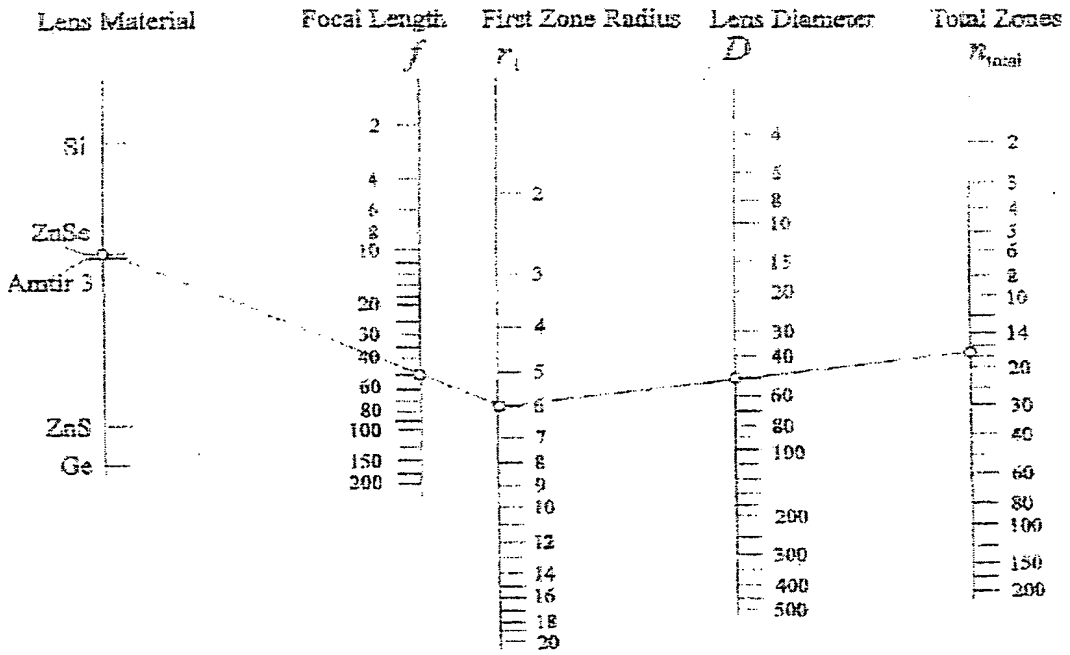

FIG. 4.27 Nomogram for hybrid achromat for the 3- to 5-μm region (object located at infinity).

This nomogram quickly assesses whether a proposed hybrid achromat requires a reasonable number of zones. For economic reasons, the tool radius is kept as large as possible in single-point diamond turning. However, the larger the tool radius, the more transmitted energy is being redirected at each zone transition step and turned into stray radiation. Fortunately, more than twenty zones are seldom needed for IR applications. The blockage, or shadowing effects, caused by the cutting tool can amount to several percent.[5]

For the 8- to 12-μm region, germanium is a superior material with its high Abbe number of almost 1,000. It is in a class of its own compared to other diamond-turnable materials. This is indicated in Fig. 4.28 by the large separation from the other materials on the material scale. An *f*/1 germanium lens with 100-mm focal length requires only three steps (four zones) across its diameter. From $\beta_{chrom} \equiv 1/[2V(f/\#)]$ one can see that for germanium, the angular chromatic blur amounts to only $0.0005/(f/\#)$ radians.

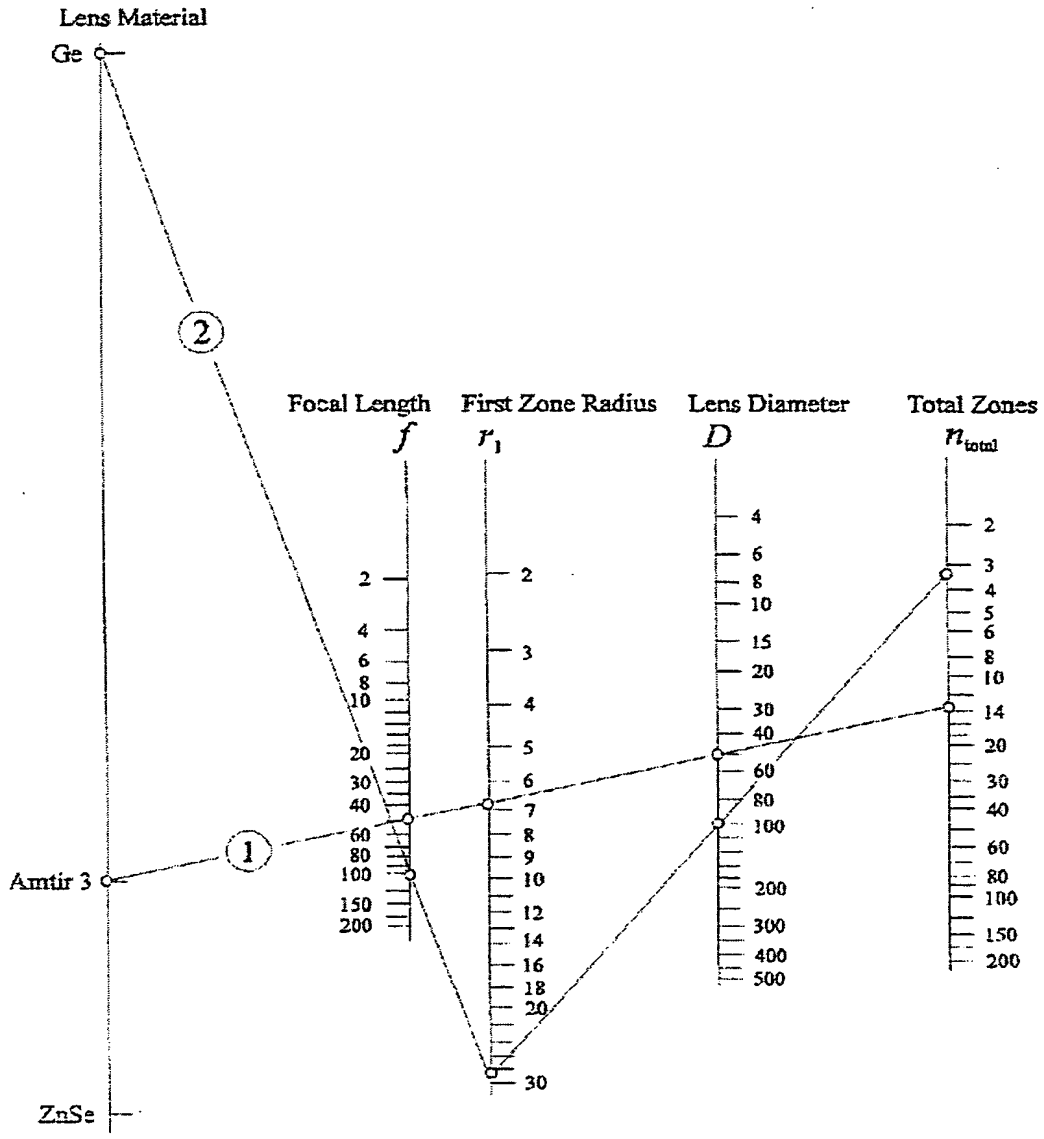

FIG. 4.28 Nomogram for hybrid achromat for the 8-to 12-μm region (object located at infinity).

In Fig. 4.28, example (1) shows an *f*/1 Amtir 3 lens with a 50-mm focal length. The first zone radius is found to be 6.7 mm, leading to a total of 14 zones across the lens diameter. The second example (2) is the *f*/1 germanium lens discussed above with a focal length of 100 mm. Here, the first radius is quite large, measuring 28.3 mm. Over the 100-mm diameter, only 4 zones are required to correct chromatic aberration.

4.5.4 Diffraction efficiency

As Eq. (4.46) indicates, the zone radii are calculated with reference to the center wavelength λ_0. At any other wavelength, detuning occurs. This means that the diffraction efficiency will be reduced.

Based on the scalar theory,[7] the diffraction efficiency for the first diffraction order is stated by

$$\mathcal{E}_1 = \left\{ \frac{\sin\left[\pi\left(\frac{\lambda_0}{\lambda} - 1\right)\right]}{\pi\left(\frac{\lambda_0}{\lambda} - 1\right)} \right\}^2 \tag{4.48}$$

Fig. 4.29 shows the diffraction efficiency $\mathcal{E}_1$ as a function of the wavelengths ratio λ_0/λ. To balance the efficiency over a given spectral band, between λ_1 and λ_2, the center wavelength should be chosen as

$$\lambda_0 = \frac{2\lambda_1\lambda_2}{\lambda_1 + \lambda_2} \tag{4.49}$$

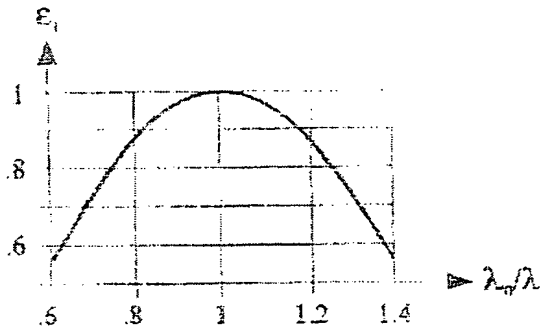

FIG. 4.29 Diffraction efficiency as a function of the ratio λ_0 and λ.

The approximate average efficiency can be stated by

$$\mathcal{E}_1 \cong 1 - \frac{\pi^2}{36}\left[\frac{\Delta\lambda}{\lambda_0}\right]^2 \tag{4.50}$$

where $\Delta\lambda = \lambda_2 - \lambda_1$.

As an example, for $\lambda_1 = 8$ and $\lambda_2 = 12$ μm, the center wavelength for equal efficiency reduction at both ends of the spectral window would be

$\lambda_0 = (2\times8\times12)/(8+12) = 9.6$ μm. With that, the average diffraction efficiency $\bar{\varepsilon}_1 \cong 95\%$. If we would have chosen 10 μm as the center wavelength instead of 9.6, the efficiency would have dropped to 81% at 8 μm and to 91% at 12 μm. The average efficiency would have stayed about the same. The shifting of the center, or blaze, wavelength can be effectively employed to favor one end of the spectral window relative to the other. This can be of interest for applications where signal strengths need to be balanced.

4.5.5 "Useful" spectral bandwidth

Rearranging Eq. (4.50) and solving for the bandwidth $\Delta\lambda$ yields

$$\Delta\lambda \cong \frac{6\lambda_0}{\pi}\sqrt{1-\bar{\varepsilon}_1}. \tag{4.51}$$

Assuming an average diffraction efficiency of 95%,

$$\Delta\lambda \cong 0.427\,\lambda_0. \tag{4.52}$$

For the LWIR region, with $\lambda_0 = 10$ μm, the "useful" bandwidth is therefore 4.27 μm. At $\lambda_0 = 4$ μm, the center of MWIR, $\Delta\lambda = 1.71$ μm, and for the visible spectrum with $\lambda_0 = 0.55$ μm, $\Delta\lambda = 0.23$ μm. These numbers reveal that over the common bandwidths, 5% or more of the radiation will be diffracted into higher orders. In other words, there will be at least 5% stray radiation, which may cause some system problems. One can also look at this from a different perspective. The stray radiation will raise the background signal level and therefore lower the contrast. This affects the modulation transfer function (MTF).[7] MTF will be covered in Chap. 6.

4.5.6 The hybrid achromat, corrected for chromatic and spherical aberrations

Changing one of the two surfaces of a singlet to an asphere will correct the lens for spherical aberration. To eliminate chromatic aberration we add the diffractive phase profile as described above. A good choice is to combine the two approaches by superimposing the phase profile onto the aspheric surface. For better protection against the environment, the second lens surface is preferred.

We remember from Eqs. (3.5) and (3.6) that a thin lens shaped for minimum spherical aberration has the following radii:

$$R_1 = \frac{2(N+2)(N-1)}{N(2N+1)}f \quad \text{and} \quad R_2 = \frac{2(N+2)(N-1)}{N(2N-1)-4}f.$$

The aspheric shape (conic section for third-order correction) of the second surface for such a basic lens is expressed by the conic constant

$$p_2 = 1 + \frac{2N(4N-1)(N+2)^2}{\left[N(2N-1)-4\right]^3} \tag{4.53}$$

For comparison, the conic constants for the four different basic materials mentioned frequently throughout this tutorial text are

Material	N	p_2	Shape
Glass	1.5	-182.75	Hyperbola
Zinc Selenide	2.4	6.9544	Ellipse
Silicon	3.4	1.6431	Ellipse
Germanium	4.0	1.3125	Ellipse

Applying these equations to the *f*/1 germanium singlet with a focal length of 100 mm, used for the 8- to 12-μm window, we correct for spherical and chromatic aberrations and find:

First radius	$R_1 = 100$ mm	Eq. (3.5)
Second radius	$R_2 = 150$ mm	Eq. (3.6)
Conic constant	$p_2 = 1.3125$	Eq. (4.53)
First zone radius	$r_1 = 28.2$ mm	Fig. 4.28 or Eq. (4.46)
Total zones required	$m_{\text{total}} = 3.14 = 4$	Fig. 4.28 or Eq. (4.47)

Using these numbers as a starting point, adding a suitable thickness and the refined, real index of refraction and optimizing the parameters with a computer yields in a matter of seconds an achromatic hybrid that does not vary too much from this thin-lens third-order-aberration-corrected singlet, even for the very low relative aperture of *f*/1. This is another verification of the thin-lens approach for the IR.

4.5.7 Binary optics

The term *binary optics* relates to the manufacturing process of a diffractive surface. In the photolithographic process the phase profile is not etched into the substrate material as a continuous surface within a given zone, but approximated with a number of steps. This is illustrated in Fig. 4.30. The relationship between the number M of photolitographic masks needed to produce K steps or levels is

$$K = 2^M . \tag{4.54}$$